Weak-link magnetically modulated resistance response in granular superconducting systems

Taner Edis

Department of Physics and Astronomy, The Johns Hopkins University, 3400 North Charles Street, Baltimore, Maryland 21218

Kishin Moorjani

Applied Physics Laboratory, The Johns Hopkins University, Johns Hopkins Road, Laurel, Maryland 20723
(Received 22 June 1994; revised manuscript received 31 August 1994)

Experimentally, magnetically modulated resistance (MMR) techniques are effective in ascertaining the properties of granular superconductors, which can be modeled as a network of Josephson junctions. Each junction is parametrized by a critical current, with a capacitance and resistance in parallel to account for the nonsupercurrent components. The overall current-voltage behavior of the network, in the presence of an external magnetic field, is given by a set of coupled nonlinear ordinary differential equations, which are studied numerically. Features of interest in the simulated experiments arise from effects of the applied field on couplings, and the transitions between multiple solution classes of the differential equations. Through these simulations of the phase dynamics, details of the weak link MMR signal can be understood, the typical signal being reproduced with large enough networks.

I. INTRODUCTION

Granularity is a common feature of superconducting materials, particularly those with high T_c, which have small and anisotropic coherence lengths so that even small scale disorder can lead to weak links. That such samples are often describable as disordered arrays of Josephson coupled grains was clear soon after these materials became available,[1] and was confirmed by subsequent experimental work as well.[2] It has proved difficult to grow good and large single crystals.

Parallel to the intense interest in high-T_c, junction arrays have an intrinsic physical interest.[3] Ordered networks have been a subject of study as oscillator arrays, focusing on features relating to coherence, stability,[4,5] and nonlinear dynamics.[6] The statistical mechanics of junction arrays have been studied, with work done on the effects of frustration,[7,8] glasslike properties,[9] and critical behavior,[10,11] focusing on the phase transition in an external magnetic field and applied current.[12]

The magnetically modulated resistance (MMR) method, being a form of modulation spectroscopy where obscured structure is uncovered by examining a derivative response,[13] has been very effective in determining the quality of superconductors,[14] particularly in revealing multiple superconducting phases,[15] and weak links[2] when present. The method consists in applying a field of the form $B_0 + B_1 \sin\omega t$, with B_1 small and $B_1 < B_0$. The resistance then is approximately

$$R(B_0 + B_1\sin\omega t, T) \simeq R(B_0, T) + \frac{\partial R}{\partial B}\bigg|_{B_0} B_1\sin\omega t . \quad (1)$$

The response is phase detected at the modulation frequency ω, picking up the derivative signal proportional to $\partial R/\partial B$ which, close to T_c, $\simeq (\partial R/\partial T)(\partial T_c/\partial B)$. Thus, a superconducting transition results in a relatively narrow *intrinsic peak,* centered around T_c with a height

proportional to $\partial R/\partial T$. Multiple phases result in multiple intrinsic peaks.[15]

The weak-link resistance produces an *extrinsic peak* below T_c, which is not proportional to $\partial R/\partial T$, but arises from the strong magnetic-field dependence of the weak-link contribution to the resistance tail. More importantly, it changes shape in a characteristic manner with the applied field strength B_0; shifting to lower temperatures, broadening and decreasing in height with increased fields (Fig. 1). It is thereby distinguishable from the intrinsic effects. Rough weak-link models reproduce much of the qualitative extrinsic peak behavior,[2] and similar modeling efforts to understand resistive tails[16] reinforce this conclusion. Under much higher fields than those employed in MMR experiments, flux pinning, creep, or flux-trapping effects are expected to produce tailing as well, even with single crystals.[17] At low fields, these effects should be negligible.

The region of the sample explored in MMR experiments depends on the frequencies of the driving currents applied to the sample. For reasons of convenience, we here consider magnetically modulated electrical resistance (MAMER), which involves the application of a dc current and measuring the voltage across the sample. Thus the overall resistance, including that arising from weak links in the current path, is probed. A further simplification in the model is gained by restricting attention to two-dimensional granular networks, analogous to thin-film studies, thereby avoiding the more complicated forms of field penetration in a three-dimensional junction network.[18]

Most discussions of resistivity in junction arrays center on the flux-lattice dynamics, particularly since the XY model is amenable to description in terms of vortex behavior and the Kosterlitz-Thouless transition.[19,20] Here, however, we do not focus on the vortices, but the grain phase dynamics, which provides a more direct approach to the weak-link resistance.

An adequate treatment of the weak-link MAMER signal will have to account for the strong coupling of junctions to one another within the network. The voltages across the junctions ($V \propto d\phi/dt$ with ϕ the macroscopic phase difference characterizing the junction) oscillate strongly, with amplitudes comparable to the average voltage. Furthermore, an additional constraint that must be taken into account, one that does not appear in studies of Josephson junctions as circuit elements (e.g., Refs. 21 and 6), is that the phases are constrained: ϕ is not an independent variable for each junction. In the London gauge, a uniform macroscopic phase θ_i is associated with each grain i, which enters into the phase difference of each junction that grain takes part in with neighboring grains; these θ_i are independent.

In studying the time evolution of the grain phases, we begin with networks containing a small number of grains,
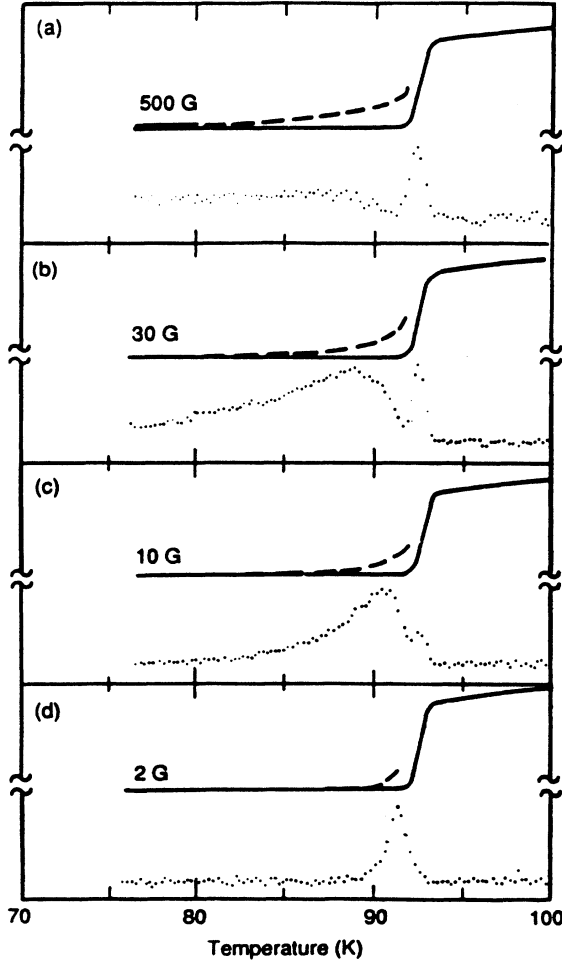

FIG. 1. The typical shifting behavior of the MAMER peak with varying magnetic fields B_0. The dotted curves are the MAMER response, the solid lines appearing above them are the dc resistance (dashed lines are ×10, in order to emphasize the tailing). On a sample of $EuBa_2Cu_3O_{7-y}$, using an external current of 5 mA. (a), (b), (c) with $B_1 = 5$ G, (d) with $B_1 = 1$ G. Taken from Ref. 2.

and cross over to larger system sizes. The results obtained from detailed network models of many grains approximate to the general case, and can be related to the understanding gained by the study of mesoscopic systems. This establishes a baseline of behavior for pure weak-link effects. There is also interest in the detailed behavior of mesoscopic networks of junctions, as highly nonlinear dynamical systems worth investigation in their own right. Such systems may also be experimentally realizable, contributing to our understanding of Josephson junction networks at the level of phase dynamics.

II. THE COUPLED JUNCTION NETWORK

To study the detailed MAMER response of a granular system, we model it as a two-dimensional randomly clustered network. In order to focus on the weak-link behavior, the intrinsic peak is included in a phenomenological manner, i.e., only junction-crossing currents meet with resistance. The external magnetic field is applied perpendicular to the plane of grains and is assumed to penetrate uniformly; the effects of fields generated by currents within the network are neglected. The geometrical complications that occur with real granular systems are absorbed within the disorder accounted for by randomly varying grain parameters. Following the McCumber model for a single junction, each contact between adjacent grains is parametrized by a normal resistance and a capacitance in parallel to an ideal Josephson junction. This allows for a realistic description that departs from the usual idealized square-lattice context; junction arrays are studied in Refs. 22–24, without involving details that would be superficial at this level of analysis.

Each of the current components through a junction can be expressed in terms of the macroscopic phase difference across the junction, ϕ_{ij}, leading to an ordinary nonlinear differential equation:

$$I_{ij} = \frac{\Phi_0}{2\pi} C_{ij} \frac{d^2\phi_{ij}}{dt^2} + \frac{\Phi_0}{2\pi} G_{ij} \frac{d\phi_{ij}}{dt} + I_{cij}\sin\phi_{ij} \qquad (2)$$

with C being the junction capacitance and G the conductance for the normal quasiparticle current.

The gauge independent form for the phase difference is

$$\phi_{ij} = \theta_i - \theta_j - A_{ij} , \qquad (3)$$

where θ is the macroscopic phase within a grain, which is spatially uniform in the London gauge. The phase shift A_{ij} is dependent on the applied magnetic field, and is important when there are junction loops, in which case it cannot be gauged away.

It proves convenient to work with dimensionless parameters; defining $i \equiv I/\mathcal{J}$, $c \equiv C/\mathcal{C}$, $g \equiv G/\mathcal{G}$, and $i_c \equiv I_c/\mathcal{J}$, where $\mathcal{J}, \mathcal{C}, \mathcal{G}$ are appropriate current, capacitance and conductance scale values for the system. The time t is rescaled as

$$\tau = \omega_c t = \frac{2\pi}{\Phi_0} \frac{\mathcal{J}}{\mathcal{G}} t \qquad (4)$$

to obtain a final form of

$$i_{ij} = \beta c_{ij}\ddot{\phi}_{ij} + g_{ij}\dot{\phi}_{ij} + i_{cij}\sin\phi_{ij} \ , \tag{5}$$

where $\dot{\phi} \equiv d\phi/d\tau$. An analog of the single junction McCumber parameter in the rescaled equation appears as $\beta = 2\pi\mathcal{J}\mathcal{C}/\Phi_0\mathcal{G}^2$. The modulation frequency will also be expressed in rescaled form, so that the applied field is $B = B_0 + B_1\sin\omega_B\tau$.

The full set of coupled ordinary differential equations (ODE's) required to specify the time evolution of the phases θ_i is obtained by current conservation on each grain i;

$$i_i^{(\text{ext})} + \sum_j i_{ij} = 0 \tag{6}$$

with $i^{(\text{ext})}$ signifying the externally applied current to a grain. The number of equations can be reduced by one, since we are free to choose an overall phase, giving $N-1$ independent equations and variables for an N grain system.

The normal capacitance and conductances, c and g, will be taken to be constant over the temperature ranges of interest. Factors that enter into the critical current and the phase shifts are where the temperature and field dependences manifest themselves. If the grains are small compared to the penetration depth, the magnetic field can be taken to be uniform in space, while the macroscopic phases remain constant within each grain. The critical current becomes

$$i_c(\Delta, T) = i_{c0}\frac{\Delta(T,B)}{\Delta(B_0)}\tanh\left[\frac{\Delta(T,B)}{2kT}\right] \tag{7}$$

with the gap parameter taken as the standard approximate Bardeen-Cooper-Schrieffer (BCS) form (assumed useful for nonzero fields also)

$$\Delta(T,B) = \Delta(B_0)\tanh(1.74\sqrt{T_c/T-1}) \tag{8}$$

with $\Delta(B_0) \simeq 1.76kT_c(B_0)$, using another BCS result extended to nonzero fields. It is sufficient for our purposes that these approximations reflect the general behavior, rather than be correct to any high accuracy. The current at $T=0$, i_{c0} can be related to the normal tunneling conductance scale as $i_{c0} \sim \pi\mathcal{G}_{\text{tunnel}}\Delta(B_0)/2e\mathcal{J}$, or fixed by determining the single junction I_c at a given temperature. The (weak) magnetic-field dependence enters through the critical temperature, $T_c(B)$. This is approximated linearly, as the modulation field B_1 is small;

$$T_c(B_0 + B_1\sin\omega_B\tau) \simeq T_c(B_0) + \frac{dT_c}{dB}\bigg|_{B_0} B_1\sin\omega_B\tau \ . \tag{9}$$

The phase shift A is straightforward for small grains,

$$A_{ij} = \frac{2\pi}{\Phi_0}\int_i^j \mathbf{A}\cdot d\mathbf{l} \ . \tag{10}$$

With grain sizes non-negligible compared to the penetration depth, which is the case of interest, the phase shifts have a more complicated dependence on the geometry. The London gauge is available, since each grain is simply connected; so in grain interiors $\mathbf{A} \propto -\mathbf{J}_s$, and the phase θ_i is uniform within each grain i. When the pair tunneling between grains is dominated by very small regions that are closest to each other, Eq. (7) can be applied directly. The other limit of interest is that of rectangular long junctions, where the full interference effects come into play through a flux-dependent modulation factor. This can have important consequences with small networks, while it is qualitatively not significant when disordered networks with large numbers of coupled grains are studied. Since the interference within mesoscopic scale networks is an interesting question, the strict rectangular limit will be considered in general.

The i_c and A expressions given for small grains can now be taken as coming into the description of infinitesimal current densities. The approximation employed will be that within each junction the magnetic field is uniform. Since the field is expelled from the interior of the grains, the effective uniform field between the grain surfaces will be significantly larger than the applied field. This can be thought of as the applied field multiplied by an "area" factor,[25] approximately the total area perpendicular to the field, $A_\perp$, divided by the area between grains that has a nonzero field, $A_{g\perp}$:

$$B_e = a_f B \sim \frac{A_\perp}{A_{g\perp}}B \ . \tag{11}$$

All previous equations dependent on B, such as Eq. (9) can be taken to depend on B_e where appropriate, with implied a_f factors. In the following, $B_{e0} = a_f B_0$ and $B_{e1} = a_f B_1$ will be used.

In the case of a rectangular junction, the dependence of the critical current on the field is well known[26] leading to the supercurrent expression

$$i_s = i_c(\Delta, T)\frac{\sin(\pi\Phi/\Phi_0)}{\pi\Phi/\Phi_0}\sin(\theta_1 - \theta_2 - A_{\text{mid}}) \tag{12}$$

for the whole junction; with A_{mid} the phase shift Eq. (10) for the midpoint of the junction, and $i_c(\Delta, T)$ being identical to that in Eq. (7).

When more than one junction exists in a loop, it is only possible to gauge away one of the A_{mid}'s by fixing a coordinate origin. Consider the case of three grains, with three rectangular junctions in between, as the simplest example of such a loop. The relationship between the appropriate A_{mid}'s for each junction will depend on the geometry. It is no longer possible to rely on a flux argument alone, as only one equation can be obtained to relate the three phase shifts,

$$\sum_{\text{loop}} \phi = A_{12} + A_{23} + A_{31} = \Phi_{\text{enclosed}} \ . \tag{13}$$

The vector potential itself must come into play, not the flux alone.

Considering the complexity and disorder of real systems, it is not meaningful to calculate detailed relationships for different geometries, only order of magnitude estimates are needed to guide parameter assignments. It will be sufficient to use Eq. (13) as a guide to assign values to phase shifts even when they are underdetermined. In any case, a degree of accuracy for phase shifts is important primarily for the study of mesoscopic networks. At larger sizes, a random phase-shift distribution becomes a

fair approximation, though our simulation accounts for the phase-sift constraints in this case also.

III. QUALITATIVE ANALYTIC RESULTS

While the complex nonlinear set of ODE's presents no practical alternative to reliance on numerical simulation, some helpful analytic results exist that are invaluable in understanding the behavior of the solutions.

The long-time average of the scaled time-dependent voltage ($v \equiv V\mathcal{G}/\mathcal{I}$) across the junctions, $v_{ij}(\tau) = \dot{\phi}_{ij}$, is of interest for the MMR response

$$\langle v_{ij} \rangle_\tau = \lim_{\tau \to \infty} \frac{\phi_{ij}(\tau)}{\tau} . \qquad (14)$$

This also means that the average voltage can be obtained from the leading term in the asymptotic expansion of the phase functions, $\theta_i \sim v_i\tau + o(\tau)$. The remainder of the expansion includes an oscillatory function, the limit cycle. However, this asymptotic series is not practically obtainable, as the v_i's are strongly dependent on the limit cycle function.

Nevertheless, some qualitative information can be obtained from the differential equations without solving them, looking at solutions that have a periodic form for the limit cycle, when the external field is constant in time:

$$\theta_i = v_i\tau + a_0^{(i)} + \sum_{n=1}^{\infty} a_n^{(i)}\cos n\omega\tau + b_n^{(i)}\sin n\omega\tau . \qquad (15)$$

From the form of equations such as Eq. (5), particularly the $\sin\phi$ term, an important condition for the existence of periodic solutions can be derived:

$$v_i = n_i\omega , \qquad (16)$$

a *single* ω giving the frequency for all oscillations. The periodic solutions are thus labeled by a string of integers, and the voltage across a junction $v_{ij} = v_i - v_j$. A periodicity index of 0 for such a voltage can be roughly taken to indicate a junction that is "superconducting," ± 1 being a "normal" oscillation, ± 2 a period doubling and so on. Work on small networks indicates that solutions with n_i being 0 or ± 1 predominate.

A solution labeled by

$$\eta = (n_1, \ldots, n_{N-1}) \qquad (17)$$

need not exist at every point in parameter space. The constant phase solution where the whole circuit is superconducting, for example, cannot exist for currents larger than a critical value. There are chaotic solutions that are not periodic; corresponding to index integers taking infinite values. The existence of chaos is expected even in small networks, since it occurs in driven single junctions,[27] and the currents within the network oscillate even if the applied current is constant.

In any case, we can expect that multiple solutions with different η values can coexist, with convergence to either being determined by the initial values of θ_i and $\dot{\theta}_i$, which were left unspecified. A significant capacitance term in Eq. (5) means that a no-passing rule and a consequent sin-

gle asymptotic limit cycle[28] does not exist.

The problem of tracing all such families of solutions, which show up as distinct branches on the I-V curves for the system, while interesting, is very computationally intensive, and not critical for understanding MMR behavior in general. Qualitatively, however, we can expect discontinuities in average voltages as a function of temperature or current, arising from jumps between different branches. Changing T means changing i_c's, and a continuous deformation of the I-V curves, leading to transitions. Studies of junction arrays have found jumps in I-V characteristics, and have interpreted them as a result of the introduction of new vortices into the array.[24] The discontinuities that are associated with transitions between different solution families are more general, as they appear in single-plaquette networks as well, where no changes in vorticity take place.

These discontinuities are readily apparent in mesoscopic systems, but tend to get averaged out into a smoother shape when the number of grains increases. The reason is most likely related to the rapid attractor crowding with increasing degrees of freedom that occurs in oscillator arrays,[6] which should be similar in this respect to granular networks, making transitions much easier, frequent, and resulting in progressively smaller discontinuities.

The important point for the simulation is the link between the frequency of the overall voltage and its average, $\langle v \rangle = n\omega$, n being an arbitrary integer, *when the applied field is constant.*

In typical experimental conditions, the modulation frequency will be much smaller than the natural frequency of the voltage oscillations: $\omega_B \ll \omega$; with ω being related to the average voltage as in Eq. (16). This is almost always the case, except when the network nears total superconductivity. In such a situation, the voltage oscillations will behave like the external field was constant over many natural periods, and will adiabatically change as the external field very slowly varies. So solutions are expected to be the appropriate limit cycles [Eq. (15)] according to the field value at that time.

We write the expected solution at a time τ_0 as

$$\theta = v(B_e)(\tau - \tau_0) + a_0(\tau_0) + p_{\omega(B_e)}(\tau - \tau_0) \qquad (18)$$

with the function p being an oscillatory part with field-dependent frequency and form, and $v(B_e)$ being the average voltage for the solution of the equations at a given time τ_0 and field $B_e(\tau_0)$, with the explicitly τ-dependent terms held constant at their value at τ_0.

We can patch the solutions for all τ_0 together by setting the "constant" a_0 in Eq. (18) appropriately, getting

$$\theta(\tau) = v(B_e(\tau))\tau - \int d\tau\, \tau \frac{dv}{d\tau} + \tilde{p}_{\omega(B_e(\tau))}(\tau) . \qquad (19)$$

Corrective terms to the oscillatory part, indicated by $\tilde{p}$, are ignored, as the high-frequency oscillation will give a negligible $\sin\omega_B\tau$ Fourier component. Corrections having to do with the induced voltage arising from an electric field $E \propto -\partial A/\partial t$ are in a similar fashion negligible on account of Eq. (19) and the fact that the applied field frequency $\omega_B \ll 1$. This expression, with constant field v

values, reproduces the correct derivative forms, so the leading asymptotic terms for the time-dependent field differential equations are derived from the time-independent solutions.

IV. SIMULATION RESULTS

The ODE's are numerically integrated at constant fields, in order to obtain the time-averaged voltage across the network. Two separate sets of θ and $\dot{\theta}$'s are kept track of, corresponding to the high and low fields $B_0 \pm B_1$; the difference between the high and low v's computed for each temperature gives a good approximation to the MAMER response.

The intrinsic peak is included in a purely phenomenological fashion, as a proper accounting for losses within grains would make the phase dynamics problem much more complicated, and would have any appreciable effect only close to T_c. Therefore, a model that has proved useful previously[2] is employed, and the intrinsic and extrinsic responses are treated as entirely independent. The intrinsic resistance is described as

$$R_i \propto [1 + e^{-\alpha(T/T_c - 1 + aB)}]^{-1} \qquad (20)$$

with adjustable parameters α and a obtained from experimental fits; the intrinsic MAMER response is $\partial R_i / \partial B |_{B_0}$.

The system will be defined by a number of parameters and scales that were introduced previously. Order of magnitude estimates useful for the simulation are obtained by reference to experimental conditions. Table I lists the relevant material parameters, with some sample values. In it, l and d are typical junction lengths and separations. The capacitance scale $\mathcal{C} \sim \epsilon l^2 / d$; $\epsilon \simeq 10\epsilon_0$ is taken here.

The scale $\mathcal{G}$ is estimated from sample resistance data

TABLE I. Sample parameter list. All values given are order of magnitude estimates that prove useful for realistic simulations.

Variable	Typical value	Units
l	1	μm
d	1	nm
$d' \simeq d + 2\Lambda$	20	nm
$a_f \simeq l/d'$	500	
$\mathcal{C}$	0.1	pF
$\mathcal{G}$	0.1	Ω^{-1}
$\mathcal{J}$	0.2	mA
$\mathcal{J}_c(0)$	2	mA
I_{ext}	0.1	mA
B_0	50	G
B_1	1	G
f_B	10	kHz
$T_c(B_{e0})$	100	K
$dT_c/dB |_{B_{e0}}$	1	mK/G

just above T_c; $\mathcal{J}$ is taken to be equal to I_c, which is about the average current through an individual grain in large experimental systems. The scale $\mathcal{J}_c(0)$ is about the average zero-temperature critical current at applied field B_0, which can be estimated from higher-temperature values, or by other means. It is typically about an order of magnitude larger than I_{ext}. With these parameters, terms in Eq. (5) are comparable in magnitude, so that neither resistive nor capacitive currents are generally negligible.

Mesoscopic grain clusters are simulated with free boundary conditions, and are generated by randomly distributing grain centers within an area, subject to the condition that they cannot be closer than a certain length, related to l. The grains themselves are formed by the Voronoi cells around these centers [see inset diagrams in Figs. 4(a) and 5(a)], which gives the length for each junction. This length l_{ij}, is used in determining individual junction parameters, based on the overall scales. A constant external current is applied to one grain on the border of the network, emerging from one opposite to it on the perimeter of the cluster.

The easiest case to study is that with three coupled grains. This is the smallest configuration with interesting behavior and I-V branch structure, and also the one where the features are most distinct, and easily computable in a fashion that allows fairly detailed understanding at the level of voltage oscillations. With the benefit of comparisons to larger grain networks, it is even possible to see the first signs of the emergence of the typical MAMER response. This is also a unique physical system; though a "Josephson triode" has been experimentally studied,[29] its analysis was in terms of triangularly arranged independent junctions as circuit elements, not coupled grains.

Figure 2 displays a sample I-V curve for the three-grain configuration, where all grains were taken to be identical for convenience in mapping out the possibilities exhaustively (differing grain parameters brings about no significant qualitative change in the picture). The features represented are the trivial fully superconducting branch, $\eta = (0,0)$; a solution that exists at all v that has a periodicity index $\eta = (1, -1)$; and a branch where one junction has a zero average voltage, "superconducting," for $\eta = (1,0)$. In between the major branches there is a region where strange oscillating behavior sets in, starting with $\eta = (2, -2)$, owing apparently to chaotic behavior. This feature consists of many small branches close to each other; detailed study of its geometry or possible fractal characteristics has been postponed for future work, since its immediate significance in understanding MAMER responses appears minimal.

The existence of multiple branches and hysteresis in the three-grain I-V curve is not surprising, as a simple branch structure and hysteresis exists for a single junction as well. In analogy to that, we can point out that the existence of a non-negligible capacitance term in the ODE's Eq. (5) is important in allowing multiple branches.[30]

The MAMER simulations on this system clearly display the discontinuities expected (Fig. 3). The most common behavior is for the oscillations close to T_c to
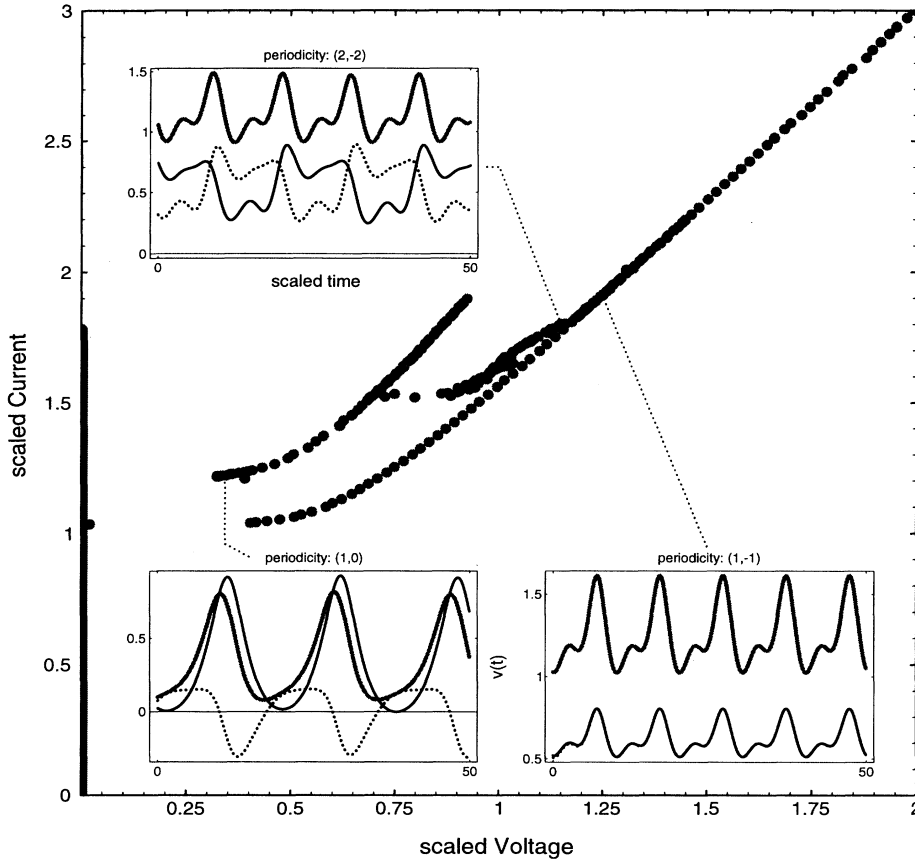
FIG. 2. I-V curve for symmetrical three-grain system. Besides the trivial superconducting branch, which is vertical, there are two main branches with $\eta = (1,0)$ and $\eta = (1,-1)$, and a feature between these that corresponds to higher periodicities and chaos. Inset are sample wave forms for the two main branches, and for when the period doubling first occurs. The voltage across each junction is shown; the time average of the voltage traced in grey is the V appearing on the I-V curves.

have a periodicity of $(1,-1)$, which become forced into a $(1,0)$ branch as the temperature is lowered, producing the initial discontinuity in the average voltage, shown in Fig. 3(a). This typically is followed by a transition to the fully superconducting state as T is decreased further, introducing a second discontinuity. There are cases where jumps to branches with higher periodicity occur, even chaos, but this is relatively uncommon. There are aspects of these plots that are of further interest. The first "peak" below T_c is showing the rudiments of the trend of shifting to lower temperatures, broadening and lessening in height, though the shape bears little resemblance to the smooth weak-link peak of experiment. This is the first sign of the MAMER weak-link response. The rest, though often large in magnitude, is entirely the result of the small system size, which allows persistence of the solution for $B_0 \pm B_1$ on a certain branch for large-T ranges. Another effect of small size is in the strong sensitivity to the applied field, and the possibility of negative MMR responses; the effects of fluxes through junctions and phase shifts are quite pronounced.

More properly mesoscopic system sizes begin to display a clearer trend towards reproducing the extrinsic peak behavior, e.g., with 20 grains. However, the consequences of small size and boundary effects manifest themselves in the unpredictable shape of the peak, sometimes including double peaks; and the clear discontinuities that

remain, though these become much smaller in size (Fig. 4). Furthermore, sensitivity to the grain configuration is present, and "peaks" at lower temperatures resulting from persistence on certain branches can occur. These peaks, though to be expected in mesoscopic systems, are spurious in terms of the extrinsic MAMER response of more realistic system sizes.

Simulations more relevant to real experiments are achieved when the number of grains exceeds $N \sim 100$, where discontinuities are washed out within the noise level, and finite size and boundary effects are reduced. Such large grain clusters are simulated with quasiperiodic boundary conditions in one direction. The grains are randomly generated on a long rectangle, $a \times b$ in dimensions, $a < b$. The shorter sides are where the external current is applied, while the long edges are identified, $y = y + a$, like on a cylinder. It must be noted that these conditions are not strictly periodic, on account of the coordinate dependence of the vector potential entering into the phase shifts. However, the effective randomization of A_{ij} at large N means problems with phase-shift constraints are not very important, while the benefit of reducing boundary effects is considerable.

With $N = 125$ (Fig. 5) the typical MAMER behavior is readily apparent: both the peak shifting behavior and the shape of the extrinsic peak closely corresponds to common experimental observations. Simulations were also
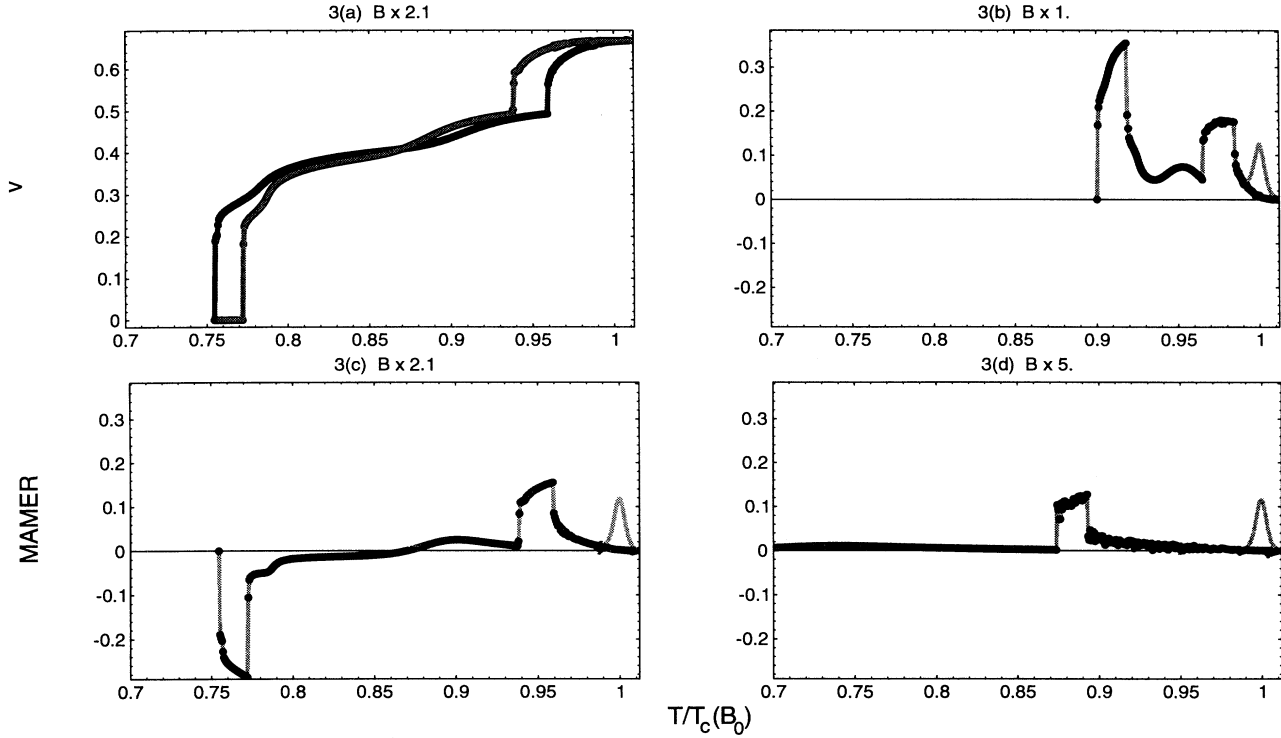
FIG. 3. Some MAMER simulations for an (asymmetric) three-grain system. The signal is derived from the difference of upper and lower field voltage averages, as with (c) being obtained from (a). The applied field B_0 increases as (b) 1, (c) 2.1, and (d) 5; scaled according to $B_0 = 1$ from Table I. Note that B_1 is not changed. Effects of the small system size are apparent, in the discontinuities, and the behavior of the spurious peaks, including a crossing to negative values in a narrow applied field range. The grey line is the overall MAMER result, including the intrinsic peak at $T/T_c(B_0) = 1$.
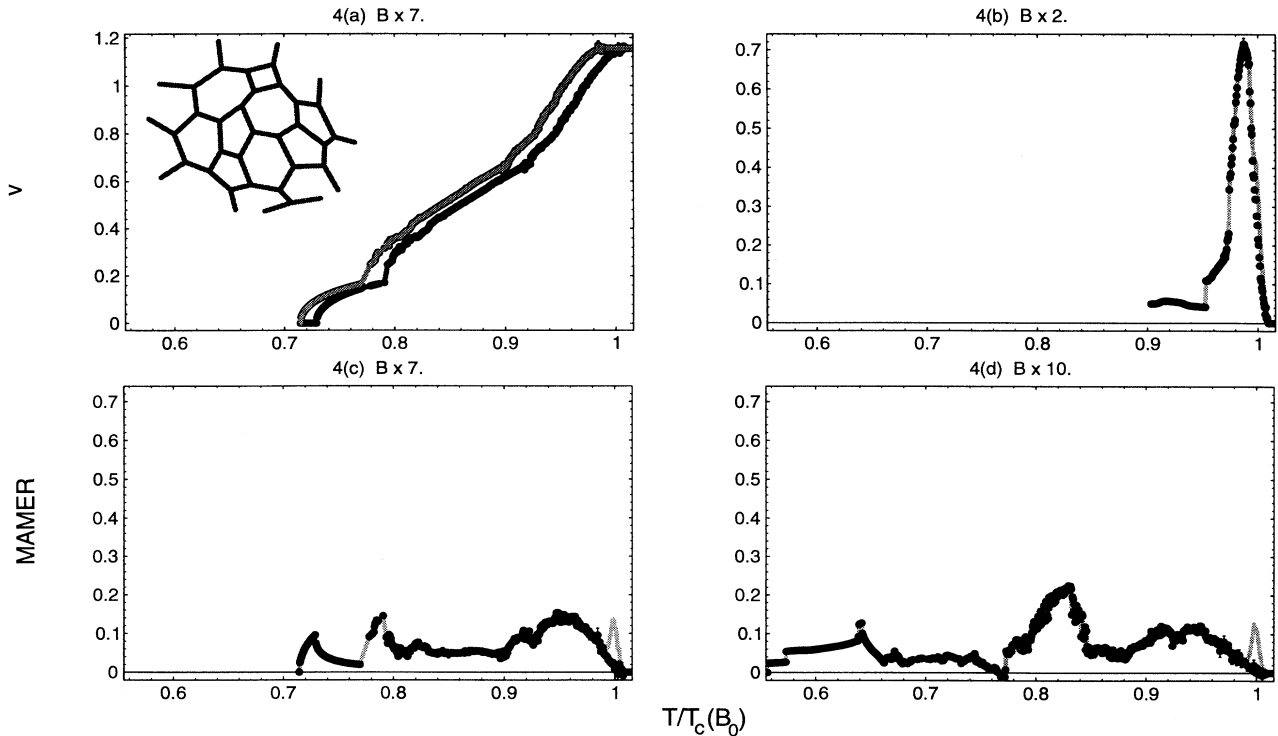

FIG. 4. MAMER simulations for a 20-grain network, depicted inset in (a), with lines representing the junctions, white space grain interiors. The signal in (c) is the difference of the $B_0 \pm B_1$ voltage averages in (a). B_0 increases as (b) 2, (c) 7, and (d) 10. Size and boundary effects are less pronounced than in Fig. 3, but clearly present, so that the typical MAMER signal and behavior with field changes have not emerged beyond a trend.
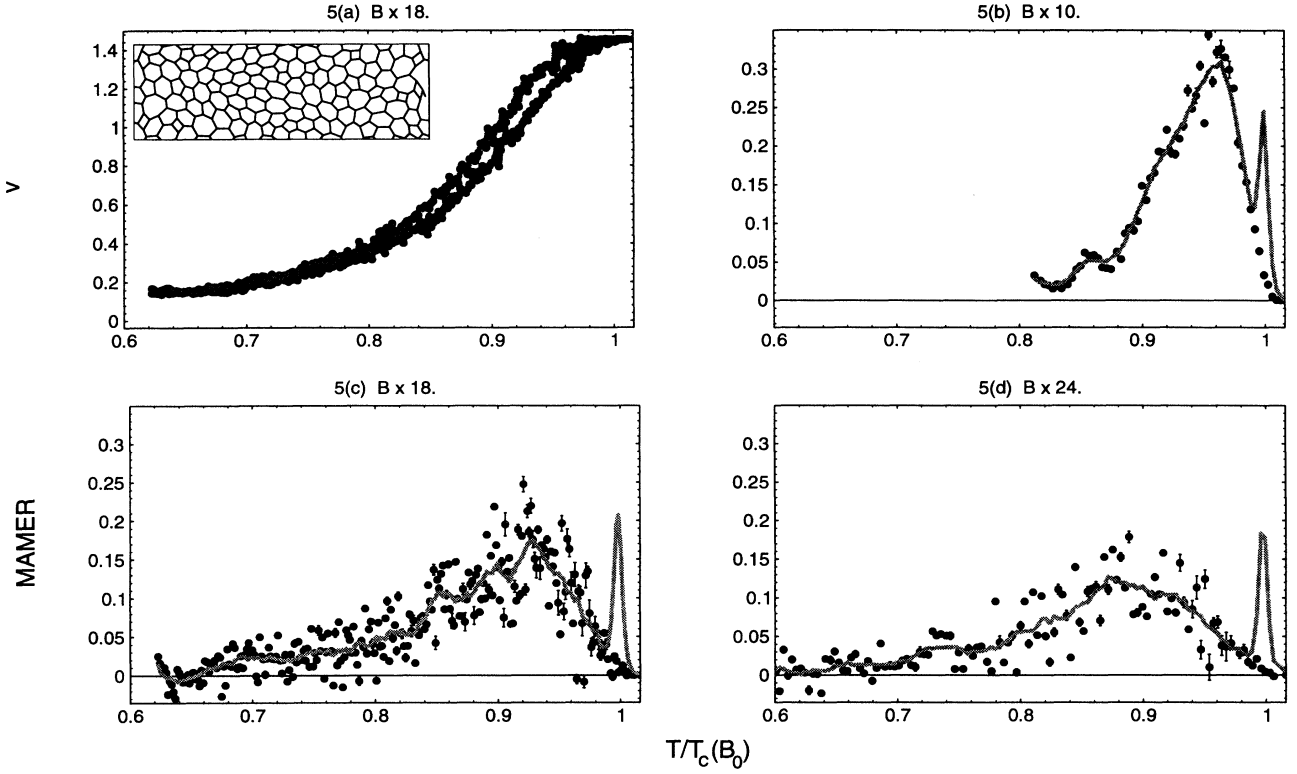
FIG. 5. Realistic behavior emerges with $N = 125$, the strip with quasiperiodic boundary conditions shown inset in (a). The plots are rather noisy, but the typical MAMER weak-link signal shape and behavior through increasing fields B_0 is present; (b) 10, (c) 18, and (d) 24. The grey line is a smoothed plot, with the initial intrinsic peak, as usual. The error bars that appear on some points come from rough error estimates relating to the stability of computed v averages.

run with networks consisting of up to 511 grains; the behavior observed differs in no significant way from that with $N = 125$. Accordingly, only results from this network are reproduced in Fig. 5, the smaller grain number reduces the computational cost and allows for a more thorough exploration of this system.

One feature of note in the simulations with larger numbers of grains is that there is an appreciable degree of noise in the computed MAMER signal. This is at a level that does not change when the size is quadrupled to $N = 511$, and spectral analysis produces no identifiable difference when different N simulations are compared. The clearest dependence of the noise amplitude on the material parameters comes through the grain size: smaller grains produce less noise. This is qualitatively in accord with experimental observation,[31] though the nature of the results does not allow direct comparison. The noise is partly on account of errors introduced by the numerical simulation, along with contributions intrinsic to the phase dynamics, such as the smaller scale branch transitions that take place. Therefore, current results pertaining to noise must remain as rough qualitative statements.

The disordered nature of the junction network should be noted in discussing these results. Ordered arrays, which attract much interest for technological reasons,

display behavior like phase-coherent solutions,[32] or even dependency on applied current direction.[33] No such effects appear in the large scale simulations; in accordance with expectations that disorder results in decreased phase coherence.[34]

V. CONCLUSIONS

The result of the simulations indicates that the typical experimental extrinsic peak in MMR studies can be reproduced by a model relying on weak-link losses alone. That this is on the basis of accounting for the complex phase dynamics of Josephson junction networks suggests that, as expected, weak links are the primary explanation for the extrinsic peak, rather than effects involving trapping of flux or other possibilities, which may indeed be important at much larger fields. While numerous simplifications have been relied on, such as a restriction to two dimensions and the more straightforward MAMER technique where MMR frequency regimes are concerned, these serve to focus on junction dynamics in detail, and do not affect the general conclusion.

Investigation of mesoscopic scale grain configurations is valuable in understanding how the extrinsic peak emerges out of phase dynamics, and in studying the crossover to typical MAMER behavior with increasing

system size, but it is conceivable that such small networks have some interest on their own. Even the simple three-grain system is not just a collection of single junctions, and has interesting features of its own; further study of it, both experimental and theoretical, should be worthwhile.

ACKNOWLEDGMENTS

[1]See, for example, D.K. Finnemore, R. N. Shelton, J. R. Clem, R. W. McCallum, H. C. Ku, R. E. McCarley, S. C. Chen, P. Klavins, and V. G. Kogan, Phys. Rev. B **35**, 5319 (1987).

[2]See, for example: B. F. Kim, J. Bohandy, T. E. Phillips, F. J. Adrian, and K. Moorjani, Physica C **161**, 76 (1989).

[3]Physica B **152**, 1 (1988). A series of articles which is still a good review of the main areas of interest in the field, though much progress has since been made.

[4]E. K. F. Dang, G. J. Halasz, and B. I. Györffy, Phys. Rev. B **46**, 8353 (1992).

[5]S. Watanabe and S. H. Strogatz, Phys. Rev. Lett. **70**, 2391 (1993).

[6]K. Wiesenfeld and P. Hadley, Phys. Rev. Lett. **62**, 1335 (1989).

[7]K. K. Mon and S. Teitel, Phys. Rev. Lett. **62**, 673 (1989).

[8]J. P. Carini, Phys. Rev. B **38**, 63 (1988).

[9]Z. Q. Wang and D. Stroud, Phys. Rev. B **44**, 9643 (1991).

[10]M. Cieplak, J. R. Banavar, M. S. Li, and A. Khurana, Phys. Rev. B **45**, 786 (1992).

[11]M. Y. Choi and D. Stroud, Phys. Rev. B **32**, 7173 (1985).

[12]F. Falo, A. R. Bishop, and P. S. Lomdahl, Phys. Rev. B **41**, 10 983 (1990).

[13]M. Cardona, in *Modulation Spectroscopy*, Solid State Physics: Advances in Research and Applications, edited by F. Seitz, D. Turnbull, and H. Ehrenreich (Academic, New York, 1969), Suppl. 11.

[14]B. F. Kim, K. Moorjani, F. J. Adrian, and J. Bohandy, in *Studies of High Temperature Superconductors*, edited by A. Narlikar (Nova Science, New York, 1992), Vol. 10, p. 63; K. Moorjani, J. Bohandy, B. F. Kim, and F. J. Adrian, in *Advances in Materials Science and Applications of High Temperature Superconductors*, edited by L. H. Bennett, Y. Flom, and K. Moorjani, NASA Conference Publication No. 3100 (NASA, Greenbelt, MD, 1991).

[15]F. J. Adrian, B. F. Kim, K. Moorjani, and J. Bohandy, Phys.

Rev. B **43**, 10 328 (1991).

[16]P. England, T. Venkatesan, X. D. Wu, A. Inam, M. S. Hedge, T. L. Cheeks, and H. G. Craighead, Appl. Phys. Lett. **53**, 2336 (1988).

[17]Y. Yeshurun and A. P. Malozemoff, Phys. Rev. Lett. **60**, 2202 (1988).

[18]John R. Clem, Physica C **162-164**, 1137 (1989).

[19]E. Granato and J. M. Kosterlitz, Phys. Rev. Lett. **62**, 823 (1989).

[20]S. Kim and M. Y. Choi, Phys. Rev. B **48**, 322 (1993).

[21]M. A. H. Nerenberg, J. H. Baskey, and J. A. Blackburn, Phys. Rev. B **36**, 8333 (1987).

[22]M. G. Forrester, S. P. Benz, and C. J. Lobb, Phys. Rev. B **41**, 8749 (1990).

[23]S. E. Korshunov, Phys. Rev. B **48**, 1124 (1993).

[24]P. L. Leath and W. Xia, Phys. Rev. B **44**, 9619 (1991).

[25]A. Gerber, Th. Grenet, M. Cyrot, and J. Beille, Phys. Rev. B **45**, 5099 (1992).

[26]T. Van Duzer and C. W. Turner, *Principles of Superconducting Devices and Circuits* (Elsevier, New York, 1981), p. 145.

[27]M. P. Sorensen, A. Davidson, N. F. Pedersen, and S. Pagano, Phys. Rev. A **38**, 5384 (1988).

[28]A. A. Middleton, Phys. Rev. Lett. **68**, 670 (1992).

[29]N. Hirose, S. Yoshimori, and M. Kawamura, Infrared Phys. **29**, 293 (1989).

[30]K. Yoshida, J. Appl. Phys. **53**, 7471 (1982).

[31]J. Bohandy, B. F. Kim, F. J. Adrian, and K. Moorjani, Phys. Rev. B **39**, 2733 (1989).

[32]H. Eikmans and J. E. van Himbergen, Phys. Rev. B **44**, 6937 (1991).

[33]L. L. Sohn, M. S. Rzchowski, J. U. Free, M. Tinkham, and C. J. Lobb, Phys. Rev. B **45**, 3003 (1992).

[34]M. Octavio, C. B. Whan, and C. J. Lobb, Appl. Phys. Lett. **60**, 766 (1992).